aerospace

MDPI

Review

High-Resolution Thermal Mapping for Quantitative UAV–TIR Applications: A Methodological Review of Sensor Integration, Calibration, and Data Processing Decisions

Kirim Lee [1] and Wonhee Lee [2,*]

[1] Research Institute of Artificial Intelligent Diagnosis Technology for Multi-Scale Organic and Inorganic Structure, Kyungpook National University, Sangju 37224, Republic of Korea; geolee@knu.ac.kr
[2] Department of Location-Based Information System, Kyungpook National University, Sangju 37224, Republic of Korea
* Correspondence: wlee33@knu.ac.kr

Abstract

Unmanned aerial vehicle (UAV)-mounted thermal infrared (TIR) sensors occupy a useful middle ground between sparse in situ measurements, occasional aircraft-based campaigns, and coarse satellite products, enabling centimeter-scale thermal mapping under field conditions. Yet converting UAV thermal imagery into quantitative temperature products remains challenging because uncooled microbolometers are radiometrically drift-prone, thermal scenes often provide weak geometric texture, and surface temperature retrieval depends on scene-specific emissivity and atmospheric assumptions. This review focuses on quantitative UAV–TIR mapping rather than on the full range of drone thermal applications. It synthesizes the technical decisions that most strongly affect the reliability, comparability, and physical interpretability of UAV-derived temperature products, from radiometric data integrity and field calibration to RGB–TIR integration, physical correction, uncertainty propagation, and validation. We clarify the literature synthesis approach, compare field-deployable calibration and drift mitigation strategies, discuss application-specific uncertainty priorities, and derive a practical reporting checklist for reproducible studies. The review emphasizes how radiometric, geometric, and physical correction choices interact, and uses comparative tables to summarize recurring trade-offs, reporting gaps, and remaining research needs. Its aim is to clarify why UAV–TIR temperature products can differ across studies and which methodological details are needed for meaningful interpretation and comparison.

Keywords: unmanned aerial vehicle; thermal infrared; land surface temperature; radiometric calibration; uncooled microbolometer; photogrammetry

Check for updates

Academic Editor: Lamei Zhang

Received: 21 March 2026
Revised: 23 April 2026
Accepted: 28 April 2026
Published: 4 May 2026

Copyright: © 2026 by the authors. Licensee MDPI, Basel, Switzerland. This article is an open access article distributed under the terms and conditions of the Creative Commons Attribution (CC BY) license.

1. Introduction

1.1. Background and Motivation

Land surface temperature (LST) is a core variable governing surface energy balance, evapotranspiration, and microclimate processes. Satellite thermal remote sensing provides global-scale LST observations and long-term continuity, but typical spatial resolution (tens of meters to kilometers) and revisit constraints limit its ability to monitor highly dynamic, fine-scale thermal phenomena that evolve over minutes to hours and over meters to tens of meters [1–4].

Ground sensors and thermal loggers provide traceable temperatures but are spatially sparse and often impractical for characterizing heterogeneous surfaces. Unmanned aerial vehicle (UAV) platforms fill this observational gap by enabling targeted acquisitions with sub-decimeter ground sampling distance and flexible timing. As UAV mapping matured, reviews documented platforms, sensors, mapping methods, and environmental monitoring practices, emphasizing the growing role of UAVs in geospatial science and operational monitoring [5–9].

The central promise of UAV–thermal infrared (TIR) sensing is not only higher spatial detail, but also the ability to resolve thermal patterns at the scale of decision-making. This includes crop canopy variability at the plant or row scale, rooftop heat loss patches at the insulation panel scale, and localized thermal anomalies associated with groundwater discharge or infrastructure defects.

1.2. Why UAV–TIR Is Different: The Quantitative Gap

Thermal mapping with UAVs is often performed for qualitative interpretation, where relative hotspots and coldspots are visually informative. However, many scientific and engineering applications require quantitative products with traceable temperatures and explicit uncertainty bounds. Precision agriculture illustrates the requirement: crop water stress assessment is sensitive to canopy temperature differences that can be smaller than uncorrected drift of uncooled cameras [10–14].

A major barrier is that most UAV thermal payloads are uncooled long-wave infrared (LWIR) microbolometers. While lightweight and power-efficient, these sensors are susceptible to temperature-dependent drift, lens self-emission changes, and radiometric discontinuities introduced by shutter-based corrections [15–17]. In addition, the conversion from measured radiance to LST requires material emissivity and corrections for reflected sky radiance and atmospheric transmission, even at low altitudes under humid conditions [18,19].

A second barrier is geometric. Many thermal scenes contain limited repeatable texture, which can destabilize image orientation in structure-from-motion (SfM) and amplify mosaic artifacts. In practice, quantitative UAV–TIR mapping requires coordinated decisions about sensor operation, calibration, flight planning, co-registration, and physics-based correction rather than treating each component in isolation [16,19].

1.3. Toward End-to-End Reproducibility

The UAV–TIR literature contains many successful demonstrations, but reported accuracies are often difficult to compare because camera settings, in-field referencing, radiative transfer assumptions, and geometric control vary substantially across studies. Small implementation details can change results, including whether radiometric imagery is used, how shutter events are handled, how emissivity is assigned by material, and how overlap regions are blended [16,17,19–21].

In UAV–TIR studies, differences in acquisition settings, calibration choices, and validation design often make reported results difficult to compare, even when similar processing tools are used. For that reason, quantitative interpretation depends on more than code availability: studies also need clear reporting of acquisition parameters, explicit distinction between brightness temperature and LST, and uncertainty information that matches the intended application. In this review, the emphasis is therefore placed on temperature products that can be interpreted and compared with confidence, rather than on mosaic appearance alone.

1.4. Positioning Relative to Existing Reviews

Several reviews cover UAV remote sensing and mapping methods across applications [5–8], UAV-based environmental monitoring practices [9], and UAV thermal sensing in specific domains such as precision agriculture [10–12]. Calibration-focused studies and best-practice discussions provide detailed guidance on radiometric limitations of uncooled microbolometers and vicarious referencing strategies [16,17,22]. Dedicated UAV–TIR LST reviews summarize retrieval models and common error sources, including emissivity and atmospheric effects [19,23,24].

Earlier reviews usually discussed calibration, geometric processing, and temperature retrieval separately. Here, these elements are considered together because, in practice, map reliability depends on how they interact during acquisition, processing, and interpretation. The contribution of this review is to bring those linked decisions into a single discussion that is more directly relevant to quantitative field use.

To clarify the specific gap addressed here, Table 1 positions the present review relative to earlier UAV and UAV–TIR review strands.

Table 1. Positioning of the present review relative to previous UAV and UAV–TIR review strands.

Review Strand (Representative Sources)	Typical Emphasis	Common Limitations for Quantitative Temperature Products	Added Value of This Review
General UAV remote sensing and mapping [5–8]	Platforms, sensors, and mapping methods across applications	Thermal radiometry, emissivity, and LST physics addressed only briefly	Thermal-specific synthesis linking radiometry, geometry, physical correction, and uncertainty reporting
UAV environmental monitoring practices [9]	Operational considerations and monitoring use cases	Temperature uncertainty and traceability rarely formalized	Uncertainty budget and reporting checklist for reproducible products
UAV thermal sensing in precision agriculture [10–12]	Canopy temperature and stress indicators in applied contexts	Cross-flight comparability and drift handling often under-specified	Calibration trade-off summary and recommendations for consistent mapping through time
Thermal camera calibration and best practices [16,17,22]	Microbolometer limitations and vicarious referencing	Often not connected to SfM stabilization and co-registration constraints	Integration of calibration with RGB–TIR fusion, geometric control, and validation design
UAV–TIR LST retrieval review [19,23,24]	Retrieval approaches and error sources	Less emphasis on reporting structure and practical mosaic diagnostics	Standardized reporting checklist and practical guidance for defensible, comparable mapping

1.5. Contributions and Paper Structure

Accordingly, this article is positioned as a methodological review of quantitative UAV–TIR mapping. Its purpose is not to provide a step-by-step operating manual or a standalone reporting standard, but to examine how radiometric, geometric, and physical correction decisions shape the reliability of UAV-derived temperature products. The tabulated summaries in the manuscript are therefore used as review-derived synthesis devices: they make cross-study assumptions, methodological trade-offs, and reporting gaps explicit, rather than prescribing a single processing procedure.

The paper is organized as follows. Section 2 reviews uncooled microbolometer behavior, radiometric data integrity, consumer- versus professional-grade payload implications, and field calibration strategies. Section 3 discusses thermal photogrammetry, RGB–TIR integration, boresight calibration, and georeferencing. Section 4 covers radiative transfer correc-

tion, emissivity assignment, application-specific uncertainty propagation, and validation, including repeated-flight consistency. Section 5 critically compares representative application domains and concludes with a cross-application synthesis of methodological trade-offs. Section 6 discusses reporting gaps, learning-based enhancement, benchmark datasets, and open research needs. Section 7 concludes with implications for standardization and quantitative UAV–TIR practice. Figure 1 summarizes the overall processing sequence.

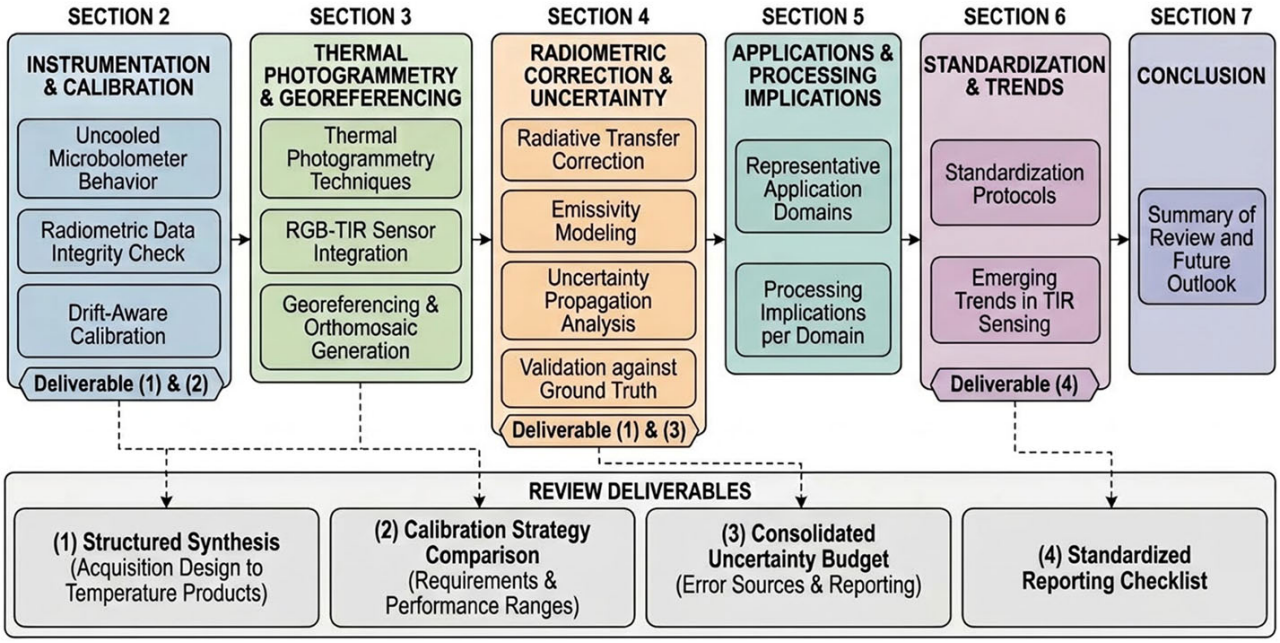

Figure 1. Structural organization of the paper: integration of the thermal remote sensing processing sequence with key review outcomes.

1.6. Scope and Terminology

To avoid ambiguity, we distinguish brightness (apparent) temperature (Tb), which is derived from sensor-measured band radiance under simplified assumptions, from surface temperature (Ts), which in the land-focused cases considered here corresponds to land surface temperature and is inferred only after emissivity, reflected downwelling radiance, and atmospheric terms are explicitly considered through a radiative transfer formulation [1,2,19,25–28].

Many UAV cameras also provide a camera-reported temperature product that depends on internal settings for emissivity, reflected temperature, atmospheric temperature, humidity, and target distance. Unless these parameters are explicitly documented and defensibly chosen, the reported temperature should be treated as an intermediate product rather than a physically validated LST estimate [16,19].

This review focuses on LWIR microbolometer cameras mounted on UAVs and on mapping methods that yield georeferenced 2D orthophotos or 3D thermal models. Shortwave infrared systems and cooled mid-wave infrared systems, while important in some industrial contexts, are outside the main scope because they involve different detector physics, calibration assumptions, and operational constraints.

1.7. Synthesis Approach and Limitations

This review focuses on quantitative UAV–TIR mapping. Rather than attempting to cover every study that has used drone thermal imagery, it emphasizes papers that report sufficient detail on acquisition design, radiometric handling, geometric control, physical correction, and validation to support technical comparison. The synthesis is

organized around the technical choices that most strongly affect quantitative temperature reliability [29,30].

The core literature search was conducted in Scopus, Web of Science, and Google Scholar. Search strings combined platform terms such as "UAV", "UAS", and "drone" with sensor and processing terms including "thermal infrared", "LWIR", "microbolometer", "thermography", "radiometric calibration", "drift", "non-uniformity correction", "flat-field correction", "land surface temperature", "emissivity", "atmospheric correction", "structure from motion", "co-registration", "uncertainty", and "validation". Backward and forward citation checks were then used to capture influential methodological papers that were not retrieved cleanly by keyword search alone.

Studies were included when they reported radiometric outputs or camera temperature products in enough detail to evaluate calibration assumptions, described geometric processing or RGB–TIR integration, discussed emissivity and/or atmospheric correction, or compared UAV-derived temperatures against independent references. Studies were excluded when they relied only on non-radiometric display imagery, reported qualitative hotspot screening without sufficient methodological detail, or duplicated already covered approaches without adding distinct technical evidence.

The cited literature base spans 1980–2026 and includes 133 sources overall. Forty cited sources were published from 2018 onward and 26 from 2020 onward, illustrating the recent growth of the field. Because the literature is highly heterogeneous in sensor type, product type (digital count (DN), radiance, Tb, or LST), reference design, environmental conditions, and evaluation metrics, the comparisons in Tables 2–5 should be read as evidence-informed technical syntheses rather than pooled meta-analytic estimates.

2. UAV–TIR Sensor Technology and Radiometric Processing

2.1. Uncooled Microbolometers: Practical Implications for UAV Mapping

Uncooled microbolometer focal-plane arrays (FPAs) detect LWIR radiation through temperature-dependent resistance changes in micro-bridge elements. Compared with cooled photon detectors, uncooled sensors exhibit stronger dependence on internal temperature and environmental conditions, which makes field accuracy drift-sensitive [15,31–33].

A key practical distinction is between sensor noise and sensor accuracy. Noise-equivalent temperature difference (NETD) describes the ability to resolve small temperature differences under stable conditions, whereas absolute accuracy depends on calibration stability, lens and housing temperature behavior, and assumptions about emissivity and atmospheric terms. In UAV deployments, these factors can dominate error budgets even when NETD is low [16,19].

Microbolometer systems also differ in shutter design, temperature stabilization, and radiometric output options. These design choices influence the frequency and magnitude of radiometric discontinuities, the availability of telemetry, and the feasibility of drift modeling [16,17].

A practical distinction also exists between consumer-grade integrated thermal payloads and professional-grade radiometric systems. Consumer-grade platforms are widely used because they simplify acquisition and reduce operational cost, but they often provide less transparent access to raw radiometric data, internal telemetry, and factory calibration details. Professional-grade systems generally offer greater control over radiometric outputs, metadata, and field recalibration procedures, which makes drift diagnosis and secondary calibration easier. This does not mean consumer systems are unsuitable for quantitative work; rather, it means that camera-reported temperatures from such platforms should be treated cautiously unless the underlying parameter settings, reference design, and field validation strategy are explicitly documented.

2.2. Measurement Chain

For interpretation, it is useful to distinguish instrument-level calibration from the later step of physical temperature retrieval. The first converts DN to band radiance or brightness temperature using camera-specific calibration, whereas the second estimates surface temperature by applying emissivity and atmospheric corrections. A camera-specific relationship converts DN to band radiance (Equation (1)) [34–36]:

$$L_band = g \cdot DN + o \quad (1)$$

Band radiance can then be mapped to brightness temperature using an inverse Planck formulation integrated over the sensor spectral response (Equation (2)):

$$Tb = B^{-1}(L_band;\ \lambda_1, \lambda_2,\ R(\lambda)) \quad (2)$$

where L_band is the band-integrated sensor radiance, g and o are camera-specific gain and offset parameters, DN denotes radiometric digital counts, B^{-1} is the inverse Planck mapping integrated over the sensor response, λ_1 and λ_2 define the lower and upper wavelength limits of the thermal band, and $R(\lambda)$ is the spectral response function. The conversion from Tb to surface temperature requires emissivity and radiative transfer correction (Section 4). In many studies, Tb is interpreted as LST without explicit correction, which can be acceptable for qualitative mapping but is insufficient for quantitative claims [19].

2.3. Radiometric Error Modes in UAV Operation

Field-deployed microbolometers commonly show drift that depends on camera-body and lens temperature. Sudden changes in airflow, solar loading, or flight dynamics can perturb lens temperature and cause step-like changes in radiometry between adjacent frames [16,17,37–39].

Shutter-based non-uniformity correction (NUC)/flat-field correction (FFC) events reduce fixed-pattern noise (FPN) and partially correct offset drift, but they can introduce discontinuities if mosaics blend frames across shutter boundaries. Lens vignetting and spatial non-uniformity can create radial temperature biases that become visible in large mosaics. Additional artifacts can arise when non-radiometric imagery is used or when in-camera contrast enhancement alters radiometric relationships [16,17].

In practice, these error sources rarely occur independently and often compound one another during mosaicking and temperature retrieval. Drift can be misinterpreted as a spatial pattern, while aggressive overlap blending can suppress true spatial gradients. A practical goal is therefore not only to reduce frame-level errors, but also to maintain mosaic consistency without removing real thermal structure.

2.4. Radiometric Data Integrity and Pre-Processing

Quantitative mapping requires radiometric outputs, typically 14–16 bit imagery or radiance products. Authors should explicitly report output type, bit depth, and any in-camera operations such as automatic gain control or histogram operations [16,17]. If only a display product is available, temperature mapping should be described as qualitative [40–42].

Pre-processing steps commonly include bad-pixel handling, optional vignette correction where supported, and flagging frames affected by shutter events. Motion blur and defocus are particularly problematic for co-registration and mosaicking. Frame screening based on blur metrics can reduce alignment failures and improve consistency, especially at higher flight speeds or under wind gusts [43].

It is also good practice to inspect radiometric histograms and saturation rates, because extreme scenes can saturate camera ranges and compress thermal contrast. For

long missions, segmentation by time blocks can help isolate drift regimes and support piecewise normalization.

2.5. Stabilization and Logging: Acquisition as Part of the Calibration

Radiometric stabilization should be planned before the flight, rather than treated as something that can be fully corrected afterward. Warm-up and thermal equilibrium behavior vary by camera and environmental conditions. Practical approaches include verifying stabilization using repeated observations of a reference target before launch, logging internal telemetry when available, and avoiding rapid changes in flight speed that can produce convective cooling effects [16,17,44–46].

Meteorological logging is important for two reasons. First, air temperature and humidity affect atmospheric transmittance and path radiance (Section 4). Second, wind and solar conditions influence true surface temperature dynamics during the flight. When surface temperatures evolve rapidly, mosaic blending can combine measurements that are not temporally comparable.

2.6. Calibration and Drift Mitigation Strategies

Calibration for UAV microbolometers is multi-layered. Factory calibration provides baseline conversion under laboratory conditions, but field drift often introduces additional offset and gain changes. Shutter-based NUC/FFC reduces spatial non-uniformity and partially stabilizes offset drift, but it does not correct emissivity, reflected radiance, or atmospheric terms [16,17,47–49].

Vicarious calibration using reference targets provides an in-field anchor for absolute temperature scales. Empirical-line methods regress camera-derived temperatures against target temperatures measured by contact sensors, enabling per-flight gain and offset adjustment [22]. Multi-target variants reduce extrapolation error by spanning the scene temperature range and can be extended to handle heterogeneous scenes by stratifying targets by material class when necessary [50].

Relative normalization methods use overlap regions to estimate inter-image offsets and reduce seam artifacts. These methods are effective for mosaic consistency but must be applied cautiously in dynamic scenes where temperature changes during acquisition. Hybrid strategies combine absolute anchoring with overlap-informed normalization to balance physical traceability and mosaic integrity [16,19]. A comparative summary of representative field-deployable radiometric calibration and drift-mitigation strategies is provided in Table 2.

Where available, absolute accuracy is expressed as root mean square error (RMSE), and mosaic consistency is expressed as overlap region temperature difference ($\mathbf{\Delta T}$). The indicative ranges in Table 2 are evidence-informed practical ranges rather than pooled estimates and are linked to representative studies in Table S1. Performance is condition-dependent: warm and humid air can widen absolute error through residual atmospheric terms, while strong solar loading or rapid convective change can increase shutter discontinuities and drift. Strategy choice should therefore be based not only on nominal accuracy, but also on mission duration, environmental stability, target logistics, and the need for cross-flight comparability.

Table 2. Radiometric calibration and drift mitigation strategies for UAV microbolometer TIR mapping *.

Strategy	Corrected Components	Absolute Anchor?	Minimum Field setup	Indicative Performance (Field)	Key Advantages	Common Cautions
Factory-only conversion baseline	DN to Tb	No	None	Absolute RMSE often 2–5 K; overlap ΔT 1–3 K	Simplest and fastest workflow	Drift dominates; poor cross-flight comparability; seam consistency often weak
Shutter NUC/FFC only	FPN + partial offset drift	No	None; shutter timing log if available	Absolute RMSE often 2–4 K; overlap ΔT 0.8–2 K	Improves fixed-pattern artifacts and visual quality	Step discontinuities at shutter events; lens and atmosphere effects remain
1–2 target empirical line (per flight)	Global gain and offset	Yes	1–2 high-emissivity targets plus traceable contact thermometer	Absolute RMSE often 1–2 K; overlap ΔT 0.5–1.5 K	Practical field anchor for absolute temperature scale	Extrapolation error if targets do not span scene temperatures; target emissivity error
Multi-target empirical line (≥3 targets)	Robust gain and offset	Yes	≥3 targets (hot/ambient/cool when feasible) plus traceable sensors	Absolute RMSE often 0.5–1.5 K; overlap ΔT 0.4–1.0 K	Reduces extrapolation and improves repeatability	Higher field logistics burden; target placement, shading, and timing matter
Multi-point variants	Robust regression; optional scene stratification	Yes	Multiple reference points or targets	Absolute RMSE often ~0.5–1.5 K (case dependent)	Flexible in heterogeneous scenes	Complex design; risk of overfitting if references are not representative
Telemetry-informed drift model + anchors	Drift linked to internal temperature + periodic anchors	Yes (periodic)	Telemetry access plus 1–2 anchor observations	Absolute RMSE often 0.7–1.5 K; overlap ΔT 0.3–1.0 K	Reduces target burden and supports longer missions	Telemetry not always available; model mismatch under rapid transients
Overlap-informed normalization (relative only)	Inter-image offsets and optional gains	No	High-overlap dataset	Absolute RMSE not defined; overlap ΔT 0.2–0.8 K	Highly effective for seam and striping reduction	Can absorb true temporal dynamics such as moving shadows or wind-driven canopy change
Hybrid: empirical line + overlap normalization	Absolute anchoring + relative consistency	Yes	2–3 targets plus high overlap	Absolute RMSE often 0.5–1.2 K; overlap ΔT 0.2–0.5 K	Often the best overall balance for mapped products	Implementation complexity; requires masking and diagnostics

* Indicative field performance ranges are synthesized from representative studies [13,14,17,22,30,37–39,50]; see Table S1 for source-linked evidence. Values are intended as practical guidance rather than pooled statistics and vary with sensor type, environmental conditions, target design, mission duration, and whether the evaluated product is radiance, brightness temperature, or physically corrected surface temperature.

2.7. Recurring Field Practices in Quantitative UAV–TIR Studies

Studies that report defensible temperatures tend to share a small set of field practices, regardless of application domain. The following points summarize recurring elements reported in quantitative UAV–TIR field studies [16,17,19,22,50–53]:

- Use radiometric outputs and document camera settings, including emissivity and atmospheric parameter settings, rather than relying on display imagery.
- Design reference targets with known emissivity and ensure they occupy sufficient pixels; measure target temperatures with traceable contact sensors and record the timing relative to image acquisition.
- Log shutter events and, where possible, internal temperatures; avoid mixing frames across major shutter boundaries without correction.
- Acquire high overlap and stable flight lines; avoid conditions that cause rapid scene temperature change or strong reflection effects on low-emissivity surfaces.
- Report both absolute accuracy against independent references and mosaic consistency measures in overlap regions.

These recommendations are not prescriptive rules, but they provide a baseline for defensible quantitative mapping and support meaningful comparison across studies.

When the scientific question involves change through time rather than a single flight, the calibration problem becomes stricter. Multi-flight or seasonal campaigns should repeat reference target observations, keep flight geometry and acquisition timing as consistent as feasible, log meteorological conditions for each campaign, and preserve the same emissivity and atmospheric parameterization unless a justified change is made. Cross-flight normalization can support consistency, but it should not replace stable physical anchors because true environmental change and sensor drift can otherwise become confounded.

A simple diagnostic framework can also help interpret common failures. Repeating seam artifacts usually indicate unresolved drift, shutter discontinuities, or over-aggressive blending; spatially smooth but flight-direction-dependent bias suggests temperature drift or vignette effects; localized RGB–TIR offsets at sharp boundaries point to boresight or timing mismatch; and edge zone anomalies near swath margins often indicate view angle effects or mixed pixels rather than true hotspots. Reporting these symptoms together with the chosen correction steps improves transparency and helps distinguish processing artifacts from genuine thermal structure.

3. Thermal Photogrammetry, RGB–TIR Fusion, and Georeferencing

3.1. Why Thermal SfM Is Fragile

SfM photogrammetry depends on stable, high-frequency texture and radiometric consistency. Thermal imagery frequently exhibits low contrast and fewer repeatable keypoints, especially over homogeneous vegetation, uniform roofs, or water surfaces. As a result, thermal-only SfM can suffer from alignment failure, weak geometry, or systematic distortions [54–57].

These limitations are amplified by the typically lower spatial resolution of thermal sensors relative to RGB cameras and by temporal changes in thermal patterns during acquisition. Even when geometric alignment succeeds, localized misregistration can smear thermal edges, which matters for anomaly detection tasks such as photovoltaic hotspot mapping and building-envelope inspection.

3.2. When Thermal-Only Reconstruction Works and When It Does Not

Thermal-only reconstruction can be viable when scenes contain persistent thermal texture, including industrial components, strong shadow boundaries, or geothermal features, and when acquisition uses very high overlap and stable camera operation. Direct georeferencing using real-time kinematic (RTK)/post-processed kinematic (PPK) positioning can reduce dependence on thermal keypoints by providing stronger pose priors [6,7,58,59].

In contrast, agricultural fields at midday, uniform asphalt surfaces, and water bodies often provide insufficient thermal texture for reliable matching. In such cases, thermal-

only processing can produce doming or warping artifacts in digital surface models and unstable mosaics. For quantitative mapping, a geometry-first strategy using RGB imagery is therefore increasingly common [60].

3.3. RGB–TIR Fusion: Geometry-First Approaches

A widely adopted solution is RGB–TIR integration, where RGB imagery provides robust geometry and camera poses and thermal frames are projected onto RGB-derived surfaces and orthophotos [60]. This approach usually depends on a rigid sensor mount and an estimate of the relative rotation and translation between the RGB and TIR sensors. In practice, however, boresight calibration is not a single method but a family of approaches with different strengths and failure modes. Related work on thermal mosaicking, image alignment, band registration, and image fusion provides the technical background for these cross-modal registration choices [61–64].

A first class of methods uses calibration boards or laboratory-style procedures to estimate the rigid transformation between sensors under controlled conditions. Their main advantage is repeatability: when the sensor mount is stable and synchronization is well characterized, they can provide clean initial parameters with limited scene dependence. Their main limitation is transferability. Parameters estimated in a laboratory or controlled setup may degrade in field use if the mount flexes, focus changes, vibration differs, or timing offsets during flight are not matched by the calibration configuration.

A second class of methods estimates alignment from homologous points or recognizable scene features observed in both modalities. These approaches are operationally attractive because they can adapt to in-flight conditions and do not always require a specialized laboratory setup. However, their performance depends strongly on the presence of shared structure across RGB and thermal imagery. In vegetation, low thermal texture, moving leaves, shadow change, or weak cross-modal contrast can make feature selection unstable, and automatic matches can fail silently when modality differences are large.

A third class of approaches relies on direct georeferencing support from RTK/global navigation satellite system (GNSS)/inertial measurement unit (IMU) observations and estimates only the residual inter-sensor alignment that remains after platform orientation is constrained. These workflows can reduce dependence on dense thermal tie points and are especially useful when thermal texture is poor. Their weakness is that navigation quality alone does not solve sensor synchronization, lever arm characterization, or mechanical stability. Poor timing or mount flex can still produce systematic pixel shifts even when the platform trajectory itself is accurate.

In practical terms, board-based methods are most useful when setup time is acceptable and the sensor rig is mechanically stable, field feature-based approaches are useful when scenes contain sharp cross-modal edges, and direct-georeferencing-supported approaches are preferable when thermal texture is weak but navigation data are strong. Across all three classes, the most defensible practice is to report the calibration environment, synchronization assumptions, residual pixel misregistration, and whether boresight parameters were re-used or re-estimated for each campaign.

3.4. Flight Planning for Thermal Photogrammetry (Practical Ranges)

Flight planning determines both geometric stability and radiometric comparability. For nadir mapping, high forward and side overlap is often necessary because thermal frames may contribute fewer stable features. Moderate and stable flight speeds reduce motion blur and limit radiometric transients associated with lens cooling. Consistent altitude improves geometric consistency and maintains stable ground-sampling distance [16,19,60,65,66].

Timing depends on the application. Pre-dawn mapping can reduce solar reflection effects and isolate thermal inertia contrasts in urban and hydrologic studies, whereas midday acquisitions may maximize canopy stress contrasts in agriculture. Regardless of timing, rapid changes in cloud cover or wind can produce spatiotemporal temperature variability that complicates mosaicking and validation.

Flights intended for quantitative mapping should be designed and documented as controlled measurements, with stable acquisition settings, recorded environmental conditions, and repeated flight geometry when temporal comparison is important.

3.5. Georeferencing and Accuracy Assessment

Geometric fidelity is prerequisite for meaningful thermal interpretation, especially for narrow anomalies and change detection. Direct georeferencing via RTK/PPK GNSS observations and an IMU can reduce the need for dense ground control and can stabilize bundle adjustment [6,7]. However, systematic biases may remain, particularly in challenging terrain or when camera models are not well constrained [67,68].

Indirect georeferencing with ground control points (GCPs) remains a common approach for high-accuracy mapping. Critically, accuracy should be reported using independent check points rather than only GCP residuals. Reported metrics should include horizontal and vertical error summaries, number and distribution of points, and camera model assumptions [6,7,54].

For thermal mapping, geometric error has radiometric consequences. Misregistration of even a few pixels can produce large apparent temperature differences at sharp edges, such as roof boundaries or water–land transitions. Therefore, co-registration accuracy should be evaluated relative to thermal pixel size, not only in meters.

3.6. Orthophoto, Seamlines, and Quality Assessment

Even with stable geometry, thermal orthophotos are vulnerable to seam artifacts driven by drift, shutter events, view angle effects, and true temperature changes during acquisition. Overlap analysis provides a practical diagnostic: residual differences in overlap regions can reveal drift segments, misregistration, or dynamic scene behavior [69,70].

Common mitigation strategies include excluding frames with severe blur, masking dynamic areas such as moving shadows or water surfaces during overlap estimation, and applying offset corrections that minimize residuals across overlaps. Automated blur screening has been shown to reduce failures and improve consistency in UAV mapping campaigns [43].

Mosaic blending should be described transparently, including whether weighted averaging, seamline selection, or per-strip normalization is used. For quantitative products, it can be informative to report both an absolute accuracy metric from reference targets and a mosaic consistency metric derived from overlaps.

3.7. Co-Registration Diagnostics and Common Pitfalls

RGB–TIR integration improves geometric stability, but it also introduces specific failure modes. If boresight parameters are estimated under one flight condition and applied under another, residual shifts may occur due to mechanical flex or timing differences. A practical diagnostic is to evaluate alignment against sharp edges in multiple parts of the scene and report average and worst-case pixel shifts [71,72].

Another pitfall arises when thermal imagery is enhanced using texture borrowed from RGB data. While such enhancement can improve visual interpretability, it can also create false edge sharpness that is not supported by thermal sampling. When enhanced products are used, authors should distinguish them from quantitative temperature products and report validation against independent references [64,73].

Common symptoms can also be interpreted diagnostically. A nearly constant scene-wide shift usually suggests boresight or lever arm bias; edge misalignment that varies across the swath often points to timing error, lens distortion mismatch, or imperfect projection geometry; and residuals that grow between flights suggest that mount stability or synchronization changed rather than that the scene itself changed. These distinctions matter because the correct remedy differs: recalibration addresses rigid offset bias, better time stamping addresses motion-induced misalignment, and scene-specific checkpoints are needed to expose projection errors that may remain invisible in global bundle statistics.

4. Physical Correction and Uncertainty Quantification

4.1. Low-Altitude Radiative Transfer and Atmospheric Terms

The sensor-measured radiance is a composite of surface emission, reflected downwelling sky radiance, and atmospheric path radiance. A common LWIR radiative transfer equation is shown in Equation (3) [74,75]:

$$L_{sensor} = \tau\varepsilon\, B(Ts) + \tau\,(1-\varepsilon)L\downarrow_sky + L\uparrow_atm \quad (3)$$

where L_{sensor} is the sensor-reaching band radiance; τ is atmospheric transmittance between the surface and the sensor; ε is surface emissivity; $B(Ts)$ is blackbody radiance at surface temperature Ts; $L\downarrow_sky$ is downwelling sky radiance reflected by the surface; and $L\uparrow_atm$ is upwelling atmospheric path radiance. The downward arrow concept denotes radiation incident on the surface from above, whereas the upward arrow denotes radiation emitted or scattered upward along the sensor path. Even at UAV altitudes, these terms need not be negligible when humidity is high, path length varies, or low-emissivity surfaces increase the contribution of reflected radiance.

In practice, researchers often adopt simplified atmospheric models when detailed profiles are unavailable. A defensible approach is to report whether atmospheric correction is applied, what inputs are used, and how sensitive results are to plausible ranges of humidity and air temperature. This reporting is especially important for intercomparison across sites and seasons.

4.2. Emissivity Estimation and Sensitivity

Emissivity is frequently the dominant systematic uncertainty in UAV–TIR LST retrieval. A practical rule of thumb is that small emissivity errors can translate to Kelvin-level LST differences depending on temperature regime and assumptions [19,76,77].

For heterogeneous scenes, a single emissivity value is rarely defensible. A practical strategy is to produce a material map from co-registered RGB imagery and assign class-specific emissivity values from spectral libraries. For vegetation, emissivity varies with species, moisture content, and canopy structure; for urban materials, emissivity and reflection behavior vary strongly among roofing membranes, concrete, asphalt, glass, and metals.

Because emissivity uncertainties are difficult to eliminate, sensitivity analysis should be treated as a minimum requirement in quantitative studies. Reporting LST under plausible emissivity ranges helps readers interpret whether observed thermal contrasts exceed uncertainty bounds.

4.3. View Angle Effects and Directional Emissivity

UAV acquisition geometry includes off-nadir angles across swaths and, in 3D mapping, oblique views. Many surfaces show directional emissivity and mixed-pixel behavior, producing apparent temperature variations with viewing geometry rather than true surface temperature [19,78,79].

In agricultural canopies, the observed temperature depends on the mixture of sunlit leaves, shaded leaves, and soil background. In urban scenes, facets and occlusions create strong view-dependent sampling. These effects motivate limiting off-nadir angles for 2D maps and adopting facet-aware 3D thermal models when vertical surfaces and complex geometry are central to the application.

4.4. Uncertainty Propagation: From Accuracy Claims to Uncertainty Products

A single accuracy value is rarely sufficient for quantitative thermal mapping; what matters is how uncertainty enters and propagates through the full processing chain. If Ts is written as a function of sensor outputs, calibration parameters, emissivity, atmospheric terms, and viewing geometry, uncertainty can be propagated using first-order sensitivity analysis or Monte Carlo simulation [19,80,81].

A practical distinction is between random uncertainty (sensor noise, short-term variability) and systematic uncertainty (emissivity bias, drift model mismatch, imperfect atmospheric correction). Map-level RMSE values can hide spatially structured errors caused by vignetting, view angle effects, and misregistration. Therefore, quantitative products benefit from reporting uncertainty summaries by material class and from providing uncertainty maps or uncertainty statistics for key regions.

Uncertainty also depends on the intended use. For anomaly detection, false positives can arise when uncertainty is comparable to anomaly magnitude; for crop stress mapping, relative patterns may remain useful even when absolute temperatures have bias. Clarifying the decision context helps justify which uncertainty metrics are most relevant.

Although the literature does not justify a single pooled percentage contribution for each uncertainty source, recurring application-specific patterns do emerge. In precision agriculture and plant phenotyping, emissivity assumptions, canopy–soil mixing, and within-flight drift often dominate because the thermal contrasts of interest can be small relative to bias in canopy temperature. In river, lake, and coastal water studies, reflected sky radiance, atmospheric correction, shoreline mixed pixels, and temporal mismatch between UAV observations and in situ references frequently become more important than small emissivity differences within water itself. In urban, building, and infrastructure applications, material-dependent emissivity, view angle effects, reflection from low-emissivity surfaces, and RGB–TIR misregistration at sharp boundaries can dominate error interpretation. In photovoltaic inspection, directional effects, irradiance variability, reflection, and sub-panel misregistration often matter as much as absolute radiometric bias because anomaly decisions are frequently threshold-based and edge-sensitive.

For that reason, uncertainty management should be application-specific rather than uniform. A study focused on canopy stress may gain more from better emissivity class separation and tighter synchronization with physiological measurements, whereas a river survey may benefit more from reflection control, bank masking, and carefully timed in situ observations. Likewise, urban facade or photovoltaic studies may benefit more from stricter view angle control and checkpoint-based co-registration diagnostics than from marginal gains in frame-level denoising. A practical uncertainty budget for UAV–TIR mapping, including dominant sources, indicative magnitudes, and reporting recommendations, is summarized in Table 3.

Table 3. Practical uncertainty budget for quantitative UAV–TIR mapping *.

Uncertainty Source	Main Character	Where it Enters the Workflow	Main Consequence	Practical Mitigation	Minimum Reporting Item
Sensor warm-up and internal thermal drift	Mostly systematic and time dependent	Raw radiometric frames; frame-to-frame consistency	Within-flight bias that can reach Kelvin-level drift if stabilization is poor	Warm-up before acquisition; repeated reference checks; telemetry-informed correction where available	Warm-up duration, stabilization criterion, telemetry use, pre-/post-flight reference readings
Shutter/NUC/FFC events	Mixed; often step-like in time	Frame sequence; striping behavior; seam formation	Frame-to-frame discontinuities and local radiometric jumps	Record event timing, inspect pre/post behavior, apply segment-wise correction when needed	Shutter interval, handling method, residual diagnostic plots
Reference target design and contact measurement	Mostly systematic if poorly designed	Absolute calibration and validation	Biased anchoring if targets are small, unstable, shaded, or poorly spanning the scene range	Use high-emissivity targets, repeated measurements, traceable contact sensors, stable placement	Target material, emissivity assumption, size in pixels, placement, sensor type, measurement timing
Emissivity assignment	Strongly systematic	Ts/LST retrieval and cross-material comparison	Often the dominant LST uncertainty; small emissivity errors can produce Kelvin-level bias	Class-based emissivity assignment, sensitivity analysis, clear distinction between Tb and Ts	Emissivity source, assigned values by class, sensitivity range, whether Tb or Ts is reported
Atmospheric correction	Mostly systematic	Ts/LST retrieval and comparison across flights or dates	Bias in absolute temperature, especially under humid or thermally variable conditions	Report atmospheric inputs explicitly and apply a consistent correction scheme	Air temperature, humidity, path-length assumption, correction model, whether correction was applied
View angle and mixed-pixel effects	Spatially structured systematic uncertainty	Swath edges, oblique views, 3D surfaces, canopy/facet mixtures	Apparent temperature variation caused by geometry rather than surface state	Limit off-nadir use for 2D maps; apply facet-aware analysis for 3D scenes; mask problematic edge zones	Use of nadir/oblique imagery, angle limits, scene geometry notes, any view angle filtering
Geometric misregistration	Spatially structured	RGB–TIR fusion, small objects, sharp boundaries	False hot/cold edges, anomaly inflation or suppression, boundary leakage between materials	Geometry-first workflow, careful boresight estimation, checkpoint-based alignment assessment	Co-registration strategy, boresight method, pixel misregistration statistics, checkpoint summary
Scene change during acquisition	Real temporal variation plus sampling error	Overlap correction, mosaicking, and validation	Real thermal change may be mistaken for drift or correction failure	Keep flights short where possible; avoid unstable conditions; mask dynamic areas during normalization	Flight duration, wind/cloud notes, illumination stability, masked dynamic regions

Table 3. *Cont.*

Uncertainty Source	Main Character	Where it Enters the Workflow	Main Consequence	Practical Mitigation	Minimum Reporting Item
Overlap-based normalization	Useful but can introduce systematic bias if over-applied	Mosaic balancing and seam correction	Improved seam consistency may be achieved at the cost of suppressing real dynamics	Use robust overlap selection, exclude dynamic zones, retain absolute anchors when possible	Residuals before/after normalization, masked areas, anchor use, normalization model
Validation design mismatch	Systematic plus sampling error	Accuracy reporting and interpretation	Over-optimistic agreement when footprint, timing, or target type do not match the thermal product	Synchronize measurements, match spatial support, separate calibration references from independent validation	Reference footprint, timing offset, number and distribution of validation sites, calibration/validation separation

* The recurring uncertainty sources summarized here are synthesized from [16–19,51–53,74–85]. Relative importance varies by application domain and end-use; the table therefore summarizes dominant mechanisms and mitigation logic rather than universal percentage contributions.

4.5. Validation: Reference Design and Metrics

Validation must match the claimed product. For Tb, validation targets should be radiometrically comparable to the camera band and should be large enough to avoid mixed pixels. For LST, reference surfaces should have well-characterized emissivity and thermal coupling. Reporting only a single global RMSE can be misleading; it is more informative to report bias and error statistics by material class and to describe the spatial representativeness of validation targets [16,17,19,82,83].

In-field references can include calibrated panels, water baths, or other controlled targets measured by contact sensors, while independent check targets support evaluation of generalization beyond the calibration points. Temporal synchronization between UAV observations and reference measurements is important in dynamic conditions. When repeated flights are performed, cross-flight consistency should be evaluated using stable reference areas or repeated target observations. Flight height, angle, speed, and time of day should be kept as consistent as the application allows, and atmospheric inputs, emissivity assignments, and camera settings should be documented identically or changed only with explicit justification. When normalization across flights is applied, the procedure should preserve absolute anchors so that genuine seasonal or management-driven temperature change is not removed together with sensor drift.

4.6. Interpreting Temperature Products for Decisions

Many UAV–TIR applications involve decisions based on thresholds or spatial patterns. For photovoltaic inspections, hotspot detection may use thresholding relative to nearby cells; for infrastructure monitoring, defects are inferred from localized anomalies relative to background. For crop stress mapping, indices derived from canopy temperature often rely on relative differences rather than absolute temperature. In all cases, interpretability depends on whether anomaly magnitude exceeds uncertainty and whether confounding factors such as reflection and view angle artifacts have been controlled [84,85].

Temperature maps are easier to interpret when they are accompanied by uncertainty information and by diagnostic layers such as view angle, shadow masks, and overlap quality indicators. Such additional layers support more robust interpretation than a single temperature mosaic.

5. Applications and Representative Use Cases

5.1. Precision Agriculture and Plant Phenotyping

Early UAV thermal studies demonstrated the value of combining thermal and multispectral data for vegetation monitoring [86]. Subsequent work has increasingly used UAV-based thermal observations for water stress assessment, where canopy temperature is interpreted in relation to transpiration, stomatal regulation, and soil moisture status [87–90]. Across these studies, the main methodological gain of UAV–TIR is not simply finer spatial resolution, but better separation of canopy and soil background, which reduces mixed-pixel bias relative to coarser airborne or satellite products. At the same time, agricultural studies are especially sensitive to radiometric comparability because the thermal contrasts associated with stress can be comparable to residual sensor drift.

Single-date studies often succeed with empirical calibration and careful canopy masking, but season-long or model-training studies impose stricter requirements. Changes in canopy architecture, irrigation timing, wind, and illumination can alter the apparent temperature field even when plant water status is unchanged. For that reason, the strongest agricultural studies combine repeatable acquisition timing, class-aware emissivity handling, stable reference targets, and validation designed around canopy scale rather than plot-average support.

Season-long mapping is particularly demanding because true crop development and environmental variability must be separated from cross-flight radiometric inconsistency [91–93]. In this context, time series value depends less on the visual smoothness of individual mosaics than on whether temperature products remain comparable across dates. Broader agricultural remote-sensing and UAV-spectroscopy reviews, together with field environmental monitoring work, similarly emphasize correction, metadata discipline, and environmental logging [94–97].

5.2. Hydrology, Rivers, and Groundwater–Surface Water Exchange

Hydrologic studies use UAV–TIR differently from agricultural studies. In rivers and streams, the objective is often to identify fine-scale temperature heterogeneity associated with groundwater inflow, tributary mixing, hyporheic exchange, or habitat structure rather than to estimate a uniform surface temperature field [98–101]. This makes spatial detail highly valuable, but it also means that shoreline mixed pixels and rapid temporal variability can dominate interpretation.

In coastal environments, thermal contrast between groundwater and surface water can reveal discharge zones and help target in situ sampling more efficiently [102]. Across the literature, the most successful river and coastal studies use flights short enough to limit surface change, target early morning or otherwise radiometrically stable periods when reflection is reduced, and pair UAV observations with synchronized in situ measurements for confirmation of groundwater or surface water contrasts.

The main limitation is that water surfaces are highly sensitive to reflected sky radiance, wind roughening, and viewing geometry. As a result, hydrologic UAV–TIR studies should be interpreted cautiously when acquisition geometry, meteorological conditions, shoreline masking, and validation timing are not reported explicitly [103].

5.3. Urban Microclimate and Urban Heat Island Studies

Urban thermal studies interpret temperature patterns in relation to material properties, sky view factor, shading, vegetation, and street canyon geometry [104–108]. Unlike homogeneous agricultural scenes, urban environments are dominated by sharp thermal boundaries and strong material variation. This makes UAV mapping attractive for neighborhood-scale thermal heterogeneity, but it also raises the penalty for even small co-registration errors.

Urban scenes also expose the limits of 2D nadir mosaics. Roof membranes, glass, metal, shaded facades, and canyon walls can all produce view-angle-dependent or reflected thermal signals that are not well represented by a single orthophoto. For that reason, the most defensible urban workflows either constrain analysis to near-nadir roof surfaces with carefully assigned emissivity classes or move toward facet-aware 3D thermal reconstruction when vertical surfaces and canyon processes are part of the research question. Recent UAV urban thermal reviews support this more geometry-aware interpretation and emphasize the importance of consistent acquisition and careful co-registration [109].

5.4. Infrastructure, Building Energy, and Photovoltaic Inspection

UAV thermal sensing supports building-energy assessment by identifying spatial patterns consistent with insulation defects, air leakage, or thermal bridges. In this domain, the relevant question is often whether localized thermal contrasts are physically interpretable, not merely whether an image appears visually sharp. Acquisition timing, wind, indoor–outdoor temperature gradient, and material emissivity therefore remain decisive because false positives can arise when those factors are not controlled [110–114].

For photovoltaic inspection, the interpretation problem is especially edge-sensitive. Hotspot thresholds are often defined relative to neighboring cells, so view angle effects, irradiance instability, reflection, and pixel leakage across module boundaries can distort anomaly magnitude even when the overall map looks clean [115]. In this application, geometry-first processing, strict angle control, and reporting of residual pixel misregistration are often as important as radiometric correction itself.

5.5. Geoscience and Hazard Monitoring

Hazard-monitoring applications differ from the preceding domains because they often prioritize safety and rapid situational awareness over perfectly controlled radiometry [116–119]. Volcanic, fire, or otherwise high-gradient scenes can exceed normal sensor dynamic ranges and can evolve during the flight faster than standard mosaic assumptions allow.

Accordingly, the most defensible interpretation in hazard settings is often conservative: short acquisition windows, saturation checks, explicit reporting of clipped or excluded areas, and separation between quick-look operational products and later quantitative analysis are more realistic than assuming that a single orthophoto fully preserves absolute temperature through time.

5.6. Cross-Application Synthesis of Methodological Trade-Offs

Viewed across application domains, the literature points to recurring methodological priorities rather than to a single transferable processing scheme. In precision agriculture, the strongest emphasis is usually placed on repeated acquisition timing, canopy–soil separation, empirical or multi-target calibration, and cross-date consistency control [87–97]. Hydrological studies place greater weight on short acquisition windows, reflection-aware viewing geometry, shoreline masking, and validation synchronized with in situ water measurements [98–103]. Urban and building applications highlight material-dependent emissivity, RGB–TIR co-registration, restricted off-nadir use for 2D products, and checkpoint-based geometric diagnostics [104–114]. Photovoltaic inspection emphasizes stable irradiance, strict viewing angle control, sharp-edge alignment, and uncertainty-aware interpretation of anomaly thresholds [113–115]. Hazard-monitoring studies, by contrast, often prioritize short acquisition windows, saturation-aware radiometric handling, and separation between operational quick-look products and later quantitative interpretation [116–119].

These differences show that calibration, physical correction, and uncertainty treatment are application-dependent methodological choices rather than fixed procedural steps.

For multi-date temperature comparison, the reviewed studies point to field anchoring, consistent parameterization, and repeated reference observations as central concerns. For localized anomaly detection within a single flight, relative consistency, edge fidelity, and transparent documentation of enhancement or thresholding steps may be more important than full LST retrieval. Table 4 summarizes these cross-application methodological priorities.

Table 4. Cross-application synthesis of methodological priorities in quantitative UAV–TIR mapping.

Application Domain	Mission Timing and Geometry	Preferred Calibration/ Normalization	Physical Correction Priority	Dominant Uncertainty Controls	Validation Emphasis
Precision agriculture	Repeatable time of day; high overlap; short-to-moderate flights	Empirical or hybrid approach with repeated references for cross-date work	Canopy–soil separation; class-aware emissivity	Drift, canopy–soil mixing, emissivity, cross-date consistency	Canopy-scale references; synchronized physiological observations
Hydrology	Short flights; reflection-aware viewing geometry; shoreline masking	Empirical anchor with conservative normalization	Reflected sky radiance and atmospheric handling	Reflection, mixed pixels, temporal mismatch	Synchronized in situ water temperature
Urban/building	Geometry-first RGB–TIR; near nadir for 2D roofs; oblique only if 3D is needed	Empirical or hybrid approach with checkpointed co-registration	Material class emissivity; view angle control	Reflection, emissivity, edge misregistration	By material class; pixel shift diagnostics
Photovoltaic inspection	Stable irradiance; strict viewing angle; sharp-edge fidelity	Hybrid or anchor-supported relative consistency	Threshold interpretation with geometric control	View angle, irradiance change, panel edge leakage	Module/cell-scale hotspot confirmation
Hazard monitoring	Very short windows; saturation-aware planning	Robust anchoring where feasible; avoid aggressive normalization	Separate quick-look from quantitative product	Dynamic range, saturation, real temporal change	Conservative interpretation; clipped-area reporting

6. Standardization and Future Trends

6.1. Reporting Gaps and Minimum Information for Cross-Study Comparability

The UAV–TIR community still lacks a reporting culture comparable to that of established satellite thermal products. Across the literature, one of the most persistent obstacles to reproducibility is not the absence of promising methods, but the uneven documentation of how data were acquired and processed. Studies often differ in camera output type, shutter handling, reference target design, atmospheric assumptions, overlap strategy, and validation timing, yet these choices are not always described clearly enough to support comparison across sites or campaigns [9,19,120–122].

Table 5 summarizes reporting items that recur as important for interpreting and comparing quantitative UAV–TIR studies. It should be read as a review-derived comparability checklist rather than as a formal protocol or complete operating procedure. The aim is to make explicit which acquisition, calibration, correction, geometric, uncertainty, and validation details are needed when studies make quantitative temperature claims.

The checklist in Table 5 should be interpreted in relation to study type. For qualitative hotspot or anomaly screening, the minimum requirement is transparent reporting of sensor/output type, acquisition context, image enhancement steps, and the logic used to define anomalies; full LST correction is not required unless absolute temperatures are claimed. For single-flight quantitative Tb or Ts mapping, calibration traceability, physical correction assumptions, and independent validation become mandatory. For multi-flight, seasonal,

or time series studies, the same items remain mandatory but must be supplemented by cross-flight consistency controls, repeated reference observations, fixed or closely matched flight geometry, and documentation of environmental comparability across dates. This distinction does not lower the reporting bar for simpler studies; it clarifies which information becomes critical once claims shift from qualitative pattern interpretation to quantitative comparison through time.

Table 5. Review-derived reporting items for reproducible and comparable quantitative UAV–TIR mapping *.

Processing Stage	Minimum Reporting (Must-Have)	Best Practice (Strongly Recommended)	Where to Place
Platform and sensor	UAV model; TIR camera model; spectral band; radiometric output type; bit depth	FPA resolution; lens field of view; NETD specification; whether raw DN, radiance, or temperature were stored	Materials and Methods (Sensor)
Stabilization	Warm-up protocol; shutter usage	Stabilization verification using a reference target or telemetry; criterion such as drift rate threshold	Methods plus diagnostics notes
Mission design	Altitude; speed; overlap; time of day; weather summary	Overlap at least 80/80% and higher for low-texture scenes; stable speed; record wind, humidity, clouds; avoid rapidly changing illumination	Materials and Methods (Acquisition)
Radiometric pre-processing	Bad-pixel handling; blur screening; shutter event handling	Vignette correction where applicable; quantify rejected frames; provide per-flight radiometric diagnostic plots	Methods plus Supplementary
Calibration (absolute)	Calibration approach; reference temperature traceability	Multiple targets spanning scene range; target size to avoid mixed pixels; repeated measurements through the flight; regression model form and coefficients	Methods plus calibration table
Drift mitigation	Whether drift was corrected and how	Telemetry-informed drift model; segment-based correction around shutter events; report residual drift statistics	Methods plus Results
Overlap-informed normalization	Whether overlap normalization was used	Robust overlap estimation; mask dynamic areas; report overlap residual statistics before and after correction	Methods plus Results
Geometry (SfM)	Software; camera model; georeferencing approach	RTK/PPK usage; GCP and checkpoint counts/distribution; horizontal and vertical accuracy summaries	Methods (Geometry)
RGB–TIR integration	Integration strategy; boresight estimation method	Boresight procedure; residual pixel misregistration statistics; synchronization assumptions and timing offsets	Methods (Integration)
Physical correction (Tb/Ts/LST)	Whether Tb or Ts/LST is reported; emissivity assumptions; atmospheric treatment	Class-based emissivity map; sensitivity analysis; atmospheric correction inputs; view angle constraints	Methods plus Discussion
Uncertainty	At least a scene-level error metric	Uncertainty propagation method; uncertainty budget table; uncertainty map statistics or region summaries	Results plus Discussion
Validation	Reference type; sampling timing	Independent validation targets; time synchronization; error metrics by material class	Results
Reproducibility	Software and parameters stated	Data/code availability statement; metadata template; processing diagram	Data Availability/Supplementary

* Reporting items are synthesized from recurring omissions and best-practice guidance in [9,16–19,120–122]. Their criticality differs by study type, especially between qualitative hotspot screening, single-flight quantitative mapping, and multi-flight/time series comparison.

6.2. Deep Learning: Denoising, Fusion, and Super-Resolution

Most studies on learning-based enhancement in UAV–TIR mapping fall into three overlapping groups. The first includes denoising and artifact reduction methods designed to suppress striping, fixed-pattern noise, or low-contrast appearance. These methods can be useful when they improve frame-to-frame consistency without altering the temperature scale, but in practice they are often evaluated primarily with generic image quality criteria rather than with traceable temperature references [123–127]. As a result, their value for quantitative UAV–TIR mapping remains context-dependent unless radiometric fidelity is tested explicitly.

The second category includes RGB-assisted fusion and super-resolution approaches, which transfer spatial detail from a higher-resolution visible image into the thermal domain [73,123–127]. Such methods can produce visually sharper outputs and may improve boundary definition for interpretation or screening. However, they also pose the greatest risk for quantitative use because visible-band texture can introduce non-thermal edges, apparent detail, or contrast patterns that the original thermal sampling does not physically support. In other words, improved visual realism should not be interpreted as evidence of improved temperature accuracy.

A third, smaller category aims more explicitly at radiometric preservation. These approaches evaluate performance against traceable temperature references, repeated target observations, or physically constrained consistency criteria rather than relying only on perceptual sharpness or structural similarity. For quantitative UAV–TIR work, this third group is the most relevant because it evaluates enhancement against measurement requirements rather than visual appearance alone. At present, however, the evidence base remains limited: relatively few studies demonstrate under field conditions that learning-based enhancement can simultaneously improve interpretability and preserve radiometric accuracy to a degree suitable for defensible temperature products [73,123–127].

This distinction has practical consequences for reporting and interpretation. If a model is used mainly for visualization, anomaly pre-screening, or qualitative interpretation, the enhanced output should be labeled accordingly and should not be presented as equivalent to a physically corrected temperature product. If a model is intended to support quantitative analysis, validation should include temperature-based error metrics, checks for bias preservation, and explicit discussion of how uncertainty changes after enhancement. For this reason, the most promising direction is not simply sharper thermal imagery, but learning-based methods whose radiometric behavior is transparent, physically interpretable, and independently validated.

6.3. Real-Time Onboard Processing and Operational Mapping

Near-real-time processing is likely to become increasingly important as UAV–TIR systems move from experimental campaigns toward operational monitoring. In practical settings, users often need immediate feedback on whether a flight is usable, whether drift is occurring, or whether a particular area should be re-flown. Lightweight onboard or edge-based processing can support these needs by producing quick-look mosaics, flagging potential drift, or identifying obvious anomalies while the platform is still in the field [128–130].

At the same time, speed introduces a new trade-off. Fast products are useful operationally, but they can lose traceability if compression, reduced numerical precision, simplified mosaicking, or approximate correction steps are introduced without documentation. In most cases, the most defensible workflow is therefore a two-stage one: a rapid product for field awareness and decision support, followed by a slower post-flight workflow in which full radiometric correction, geometric refinement, and validation are applied.

The key point is not to reject onboard processing, but to keep operational convenience separate from final quantitative interpretation.

6.4. Benchmark Datasets and Community Inter-Comparison

Progress in UAV–TIR methodology is still hard to evaluate because the field lacks shared benchmark datasets. At present, many new methods are tested on different cameras, different environments, different calibration designs, and different validation targets. Under those conditions, it becomes difficult to tell whether an apparent improvement reflects a genuinely better method or simply a more favorable dataset [131–133].

At this stage, additional datasets alone are not enough; what matters more is whether methods can be evaluated on datasets acquired, corrected, and validated in comparable ways. A useful benchmark should include raw radiometric imagery, metadata on camera settings and shutter events, reference target logs, meteorological observations, and reliable geometry. It should also cover several scene types, including vegetation, urban materials, water, and infrastructure, and it should include both calibration and independent validation references. With such datasets, the community could compare methods on a common basis using tasks such as absolute temperature accuracy, mosaic consistency, co-registration quality, and uncertainty reporting. Benchmarking would be especially valuable for evaluating learning-based enhancement methods, which are otherwise difficult to assess beyond visual appearance.

Benchmarking should also be tied to reporting standards. A useful community dataset would be incomplete if it provided only imagery without calibration metadata, shutter logs, geometry diagnostics, environmental observations, and independent validation measurements. Benchmark datasets and reporting practice should therefore be developed together, because the metadata needed for reproducibility are also needed for fair comparison across methods.

6.5. Open Challenges

Table 6 summarizes the main open issues in terms of data, method, and validation gaps. The first gap concerns emissivity assignment in heterogeneous scenes: current workflows often rely on class-level lookup values, but they still lack reliable ways to represent weathering, moisture change, sub-pixel mixtures, and directional effects. A concrete research priority is therefore the development of benchmark scenes with co-registered material maps, reference emissivity measurements, and sensitivity-aware LST evaluation.

The second gap concerns normalization in dynamic scenes. Existing overlap-based methods can suppress seam artifacts, but they can also remove genuine thermal change when wind, shadow motion, or rapid surface evolution occurs during acquisition. What is still missing are methods that jointly model sensor drift, scene dynamics, and uncertainty, ideally supported by repeated reference observations and community benchmark datasets for long-flight or time series conditions.

The third gap concerns directional effects in 3D thermal mapping. Current approaches often project thermal data onto 2D products even when view angle anisotropy, facet occlusion, and mixed visibility are central to the thermal signal. Progress here will likely require multi-angle acquisition design, facet-aware thermal models, and validation protocols that treat geometry and radiometry as coupled rather than separate problems.

A cross-cutting gap is the scarcity of inter-comparable datasets and reporting standards. Without traceable metadata on calibration, geometry, environmental conditions, and validation, even promising new methods remain difficult to evaluate outside their original case studies.

Table 6. Research gaps in quantitative UAV–TIR mapping: unresolved challenges, current limitations, and possible future directions.

Open Challenge	Current Limitation	What is Missing	Possible Future Directions
Emissivity assignment in heterogeneous scenes	Class-level lookup values often ignore weathering, moisture change, sub-pixel mixtures, and directional behavior	Co-registered emissivity references and sensitivity-aware benchmark scenes	Build benchmark sites with material maps, reference emissivity measurements, and LST sensitivity tests
Normalization in dynamic scenes	Overlap correction can remove real thermal change together with drift	Joint drift-scene models with uncertainty accounting	Develop anchor-supported normalization methods for long flights and time series campaigns
Directional effects in 3D thermal mapping	2D products often underrepresent anisotropy, occlusion, and facet dependence	Multi-angle acquisition and facet-aware validation	Design multi-angle surveys and evaluate geometry–radiometry coupling explicitly
Benchmark scarcity and uneven reporting	Methods remain difficult to compare across studies	Shared datasets with traceable metadata and validation targets	Establish community benchmark datasets and reporting templates

7. Conclusions

UAV thermal remote sensing is increasingly being used not only for visual hotspot detection, but also for temperature mapping intended to support scientific interpretation and engineering decisions. The literature reviewed here shows that such use is credible only when radiometric handling, geometric registration, and physical temperature interpretation are treated as parts of the same measurement problem. Across applications, the same limitations recur: radiometric drift in uncooled microbolometers, weak thermal texture for stable reconstruction, incomplete treatment of emissivity and atmospheric effects, and inconsistent reporting of acquisition and validation conditions.

From the radiometric perspective, the most reliable studies are those that treat field acquisition itself as part of the calibration strategy. The use of radiometric outputs, explicit documentation of shutter behavior, traceable reference targets, and drift-aware correction generally matters more than the visual smoothness of the final mosaic. From the geometric perspective, thermal-only reconstruction remains scene-dependent and often unstable, particularly over low-texture surfaces such as homogeneous vegetation, asphalt, roofs, and water. In many practical cases, RGB-supported geometry followed by careful RGB–TIR co-registration provides a more dependable basis for quantitative mapping. Physical interpretation is equally important. Brightness temperature, camera-reported temperature, and physically corrected surface temperature should not be treated as interchangeable products, and uncertainty should be reported in a form that reflects material class, viewing geometry, and intended use.

This review has focused on the technical decisions that most strongly affect the quality and comparability of UAV–TIR products. The comparison of calibration options, the uncertainty budget, the cross-application synthesis of methodological priorities, the reporting items, and the research gap synthesis are intended to support clearer interpretation across domains rather than to prescribe a single universal procedure. These elements should therefore be read as analytical syntheses of reported practice and recurring omissions, not as a standalone technical manual. Different applications impose different priorities. Agriculture, hydrology, urban mapping, photovoltaic inspection, and hazard monitoring

do not fail for the same reasons, and they should not be processed or evaluated as though they do.

Several needs emerge repeatedly from the literature. First, broader access to raw radiometric data and internal telemetry would improve both drift diagnosis and secondary calibration. Second, benchmark datasets with traceable reference observations, complete metadata, and well-documented acquisition conditions are needed if competing methods are to be compared on common ground. Third, reporting practice must become more consistent, particularly for camera output type, calibration assumptions, co-registration quality, environmental conditions, and validation design. In this respect, the field would benefit from a shared reporting standard built around the core reporting elements summarized in this review, together with benchmark datasets that allow calibration, mosaicking, co-registration, and uncertainty-reporting methods to be evaluated under comparable conditions. Learning-based image enhancement may become more useful in this field, but only when its radiometric behavior is transparent and independent temperature validation is treated as essential rather than optional.

UAV–TIR mapping is now constrained less by a lack of applications than by uneven control and reporting of measurement quality. Further progress will depend less on isolated demonstrations and more on shared community expectations for calibration, validation, uncertainty description, and data comparability. The establishment of community reporting standards and openly comparable benchmark resources would be an important step toward making UAV thermal mapping more reproducible, more transferable across studies, and more credible as a quantitative remote sensing methodology.

Supplementary Materials: The following supporting information can be downloaded at: https://www.mdpi.com/article/10.3390/aerospace13050430/s1, Table S1 compiles representative reported accuracy and stability metrics used to inform the indicative field performance ranges in Table 2. These studies differ in platform, sensor, environmental conditions, reference design, and evaluated product type; accordingly, Table S1 is intended to document evidential support rather than to imply strict cross-study equivalence.

Author Contributions: Conceptualization, K.L.; methodology, K.L.; software, K.L.; formal analysis, K.L.; writing—original draft preparation, K.L.; writing—review and editing K.L. and W.L.; funding acquisition, K.L. and W.L. All authors have read and agreed to the published version of the manuscript.

Funding: This work was supported by the National Research Foundation of Korea (NRF) grant funded by the Korea government (MSIT) (RS-2021-NR060108 and RS-2026-25472000).

Data Availability Statement: This can be provided upon request.

Conflicts of Interest: The authors declare no conflicts of interest.

Abbreviations

The following abbreviations are used in this manuscript:

UAV	Unmanned aerial vehicle
TIR	Thermal infrared
LST	Land surface temperature
LWIR	Long-wave infrared
SfM	Structure-from-motion
Tb	Brightness (apparent) temperature
Ts	Surface temperature
NETD	Noise-equivalent temperature difference
DN	Digital count
NUC	Non-uniformity correction

FFC	Flat-field correction
FPN	Fixed-pattern noise
RTK	Real-time kinematic
PPK	Post-processed kinematic
RGB	Red, green, and blue
GNSS	Global navigation satellite system
IMU	Inertial measurement unit
GCP	Ground control point
RMSE	Root mean square error

References

1. Li, Z.-L.; Tang, B.-H.; Wu, H.; Ren, H.; Yan, G.; Wan, Z.; Trigo, I.F.; Sobrino, J.A. Satellite-derived land surface temperature: Current status and perspectives. *Remote Sens. Environ.* **2013**, *131*, 14–37. [CrossRef]
2. Sobrino, J.A.; Jiménez-Muñoz, J.C.; Paolini, L. Land surface temperature retrieval from LANDSAT TM 5. *Remote Sens. Environ.* **2004**, *90*, 434–440. [CrossRef]
3. Wan, Z.; Dozier, J. A generalized split-window algorithm for retrieving land-surface temperature from space. *IEEE Trans. Geosci. Remote Sens.* **1996**, *34*, 892–905. [CrossRef]
4. Voogt, J.A.; Oke, T.R. Thermal remote sensing of urban climates. *Remote Sens. Environ.* **2003**, *86*, 370–384. [CrossRef]
5. Yao, H.; Qin, R.; Chen, X. Unmanned Aerial Vehicle for Remote Sensing Applications—A Review. *Remote Sens.* **2019**, *11*, 1443. [CrossRef]
6. Colomina, I.; Molina, P. Unmanned aerial systems for photogrammetry and remote sensing: A review. *ISPRS J. Photogramm. Remote Sens.* **2014**, *92*, 79–97. [CrossRef]
7. Nex, F.; Remondino, F. UAV for 3D mapping applications: A review. *Appl. Geomat.* **2014**, *6*, 1–15. [CrossRef]
8. Pajares, G. Overview and Current Status of Remote Sensing Applications Based on Unmanned Aerial Vehicles (UAVs). *Photogramm. Eng. Remote Sens.* **2015**, *81*, 281–330. [CrossRef]
9. Tmušić, G.; Manfreda, S.; Aasen, H.; James, M.R.; Gonçalves, G.; Ben-Dor, E.; Brook, A.; Polinova, M.; Arranz, J.J.; Mészáros, J.; et al. Current Practices in UAS-based Environmental Monitoring. *Remote Sens.* **2020**, *12*, 1001. [CrossRef]
10. Maes, W.H.; Steppe, K. Perspectives for Remote Sensing with Unmanned Aerial Vehicles in Precision Agriculture. *Trends Plant Sci.* **2019**, *24*, 152–164. [CrossRef]
11. Xie, C.; Yang, C. A review on plant high-throughput phenotyping traits using UAV-based sensors. *Comput. Electron. Agric.* **2020**, *178*, 105731. [CrossRef]
12. Guebsi, R.; Mami, S.; Chokmani, K. Drones in Precision Agriculture: A Comprehensive Review of Applications, Technologies, and Challenges. *Drones* **2024**, *8*, 686. [CrossRef]
13. Mesas-Carrascosa, F.-J.; Pérez-Porras, F.; Meroño de Larriva, J.E.; Mena Frau, C.; Agüera-Vega, F.; Carvajal-Ramírez, F.; Martínez-Carricondo, P.; García-Ferrer, A. Drift Correction of Lightweight Microbolometer Thermal Sensors On-Board Unmanned Aerial Vehicles. *Remote Sens.* **2018**, *10*, 615. [CrossRef]
14. Aragon, B.; Johansen, K.; Parkes, S.; Malbeteau, Y.; Al-Mashharawi, S.; Al-Amoudi, T.; Andrade, C.F.; Turner, D.; Lucieer, A.; McCabe, M.F. A Calibration Procedure for Field and UAV-Based Uncooled Thermal Infrared Instruments. *Sensors* **2020**, *20*, 3316. [CrossRef]
15. Budzier, H.; Gerlach, G. *Thermal Infrared Sensors: Theory, Optimisation and Practice*; Wiley: Chichester, UK, 2011.
16. Kelly, J.; Kljun, N.; Olsson, P.-O.; Mihai, L.; Liljeblad, B.; Weslien, P.; Klemedtsson, L.; Eklundh, L. Challenges and Best Practices for Deriving Temperature Data from an Uncalibrated UAV Thermal Infrared Camera. *Remote Sens.* **2019**, *11*, 567. [CrossRef]
17. Maguire, M.S.; Neale, C.M.U.; Woldt, W.E. Improving Accuracy of Unmanned Aerial System Thermal Infrared Remote Sensing for Use in Energy Balance Models in Agriculture Applications. *Remote Sens.* **2021**, *13*, 1635. [CrossRef]
18. Berk, A.; Hawes, F. Validation of MODTRAN®6 and its line-by-line algorithm. *J. Quant. Spectrosc. Radiat. Transf.* **2017**, *203*, 542–556. [CrossRef]
19. Ndlovu, H.S.; Odindi, J.; Sibanda, M.; Mutanga, O. A systematic review on the application of UAV-based thermal remote sensing for assessing and monitoring crop water status in crop farming systems. *Int. J. Remote Sens.* **2024**, *45*, 4923–4960. [CrossRef]
20. Anderson, K.; Gaston, K.J. Lightweight unmanned aerial vehicles will revolutionize spatial ecology. *Front. Ecol. Environ.* **2013**, *11*, 138–146. [CrossRef]
21. Hardin, P.J.; Jensen, R.R. Small-Scale Unmanned Aerial Vehicles in Environmental Remote Sensing: Challenges and Opportunities. *GISci. Remote Sens.* **2011**, *48*, 99–111. [CrossRef]
22. Torres-Rua, A. Vicarious Calibration of sUAS Microbolometer Temperature Imagery for Estimation of Radiometric Land Surface Temperature. *Sensors* **2017**, *17*, 1499. [CrossRef]

23. Messina, G.; Modica, G. Applications of UAV Thermal Imagery in Precision Agriculture: State of the Art and Future Research Outlook. *Remote Sens.* **2020**, *12*, 1491. [CrossRef]
24. Lee, K.; Lee, W.H. Temperature Accuracy Analysis by Land Cover According to the Angle of the Thermal Infrared Imaging Camera for Unmanned Aerial Vehicles. *ISPRS Int. J. Geo-Inf.* **2022**, *11*, 204. [CrossRef]
25. Li, Z.-L.; Becker, F. Feasibility of land surface temperature and emissivity determination from AVHRR data. *Remote Sens. Environ.* **1993**, *43*, 67–85. [CrossRef]
26. Norman, J.M.; Becker, F. Terminology in thermal infrared remote sensing of natural surfaces. *Agric. For. Meteorol.* **1995**, *77*, 153–166. [CrossRef]
27. Norman, J.M.; Kustas, W.P.; Humes, K.S. A two-source approach for estimating soil and vegetation energy fluxes in observations of directional radiometric surface temperature. *Agric. For. Meteorol.* **1995**, *77*, 263–293. [CrossRef]
28. Kustas, W.P.; Norman, J.M. Evaluation of soil and vegetation heat flux predictions using a simple two-source model with radiometric temperatures for partial canopy cover. *Agric. For. Meteorol.* **1999**, *94*, 13–29. [CrossRef]
29. Aubrecht, D.M.; Helliker, B.R.; Goulden, M.L.; Roberts, D.A.; Still, C.J.; Richardson, A.D. Continuous, long-term, high-frequency thermal imaging of vegetation: Uncertainties and recommended best practices. *Agric. For. Meteorol.* **2016**, *228–229*, 315–326. [CrossRef]
30. Elfarkh, J.; Johansen, K.; Angulo, V.; Camargo, O.L.; McCabe, M.F. Quantifying Within-Flight Variation in Land Surface Temperature from a UAV-Based Thermal Infrared Camera. *Drones* **2023**, *7*, 617. [CrossRef]
31. Rogalski, A. Recent progress in infrared detector technologies. *Infrared Phys. Technol.* **2011**, *54*, 136–154. [CrossRef]
32. Nugent, P.W.; Shaw, J.A.; Pust, N.J. Correcting for focal-plane-array temperature dependence in microbolometer infrared cameras lacking thermal stabilization. *Opt. Eng.* **2013**, *52*, 061304. [CrossRef]
33. Budzier, H.; Gerlach, G. Calibration of uncooled thermal infrared cameras. *J. Sens. Sens. Syst.* **2015**, *4*, 187–197. [CrossRef]
34. Schott, J.R. *Remote Sensing: The Image Chain Approach*; Oxford University Press: New York, NY, USA, 2007. [CrossRef]
35. Rees, W.G. *Physical Principles of Remote Sensing*, 3rd ed.; Cambridge University Press: Cambridge, UK, 2013. [CrossRef]
36. Slater, P.N. *Remote Sensing: Optics and Optical Systems*; Addison-Wesley Publishing Company: Reading, MA, USA, 1980.
37. Han, X.; Thomasson, J.A.; Swaminathan, V.; Wang, T.; Siegfried, J.; Raman, R.; Rajan, N.; Neely, H. Field-Based Calibration of Unmanned Aerial Vehicle Thermal Infrared Imagery with Temperature-Controlled References. *Sensors* **2020**, *20*, 7098. [CrossRef]
38. Acorsi, M.G.; Gimenez, L.M.; Martello, M. Assessing the Performance of a Low-Cost Thermal Camera in Proximal and Aerial Conditions. *Remote Sens.* **2020**, *12*, 3591. [CrossRef]
39. Niwa, H. Comparison of the accuracy of two UAV-mounted uncooled thermal infrared sensors in predicting river water temperature. *River Res. Appl.* **2022**, *38*, 1660–1667. [CrossRef]
40. Abràmoff, M.D.; Magalhães, P.J.; Ram, S.J. Image Processing with ImageJ. *Biophotonics Int.* **2004**, *11*, 36–42.
41. Metsu, C.; Maes, W.H.; Ottoy, S.; Van Meerbeek, K. theRmalUAV: An R package to clean and correct thermal UAV data for accurate land surface temperatures. *Methods Ecol. Evol.* **2026**, *17*, 488–496. [CrossRef]
42. FLIR Systems, Inc. *FLIR Vue Pro and Vue Pro R User Guide*; FLIR Systems, Inc.: Wilsonville, OR, USA, 2016.
43. Ribeiro-Gomes, K.; Hernández-López, D.; Ballesteros, R.; Moreno, M.A. Approximate Georeferencing and Automatic Blurred Image Detection to Reduce the Costs of UAV Use in Environmental and Agricultural Applications. *Biosyst. Eng.* **2016**, *151*, 308–327. [CrossRef]
44. Olbrycht, R.; Więcek, B.; De Mey, G. Thermal drift compensation method for microbolometer thermal cameras. *Appl. Opt.* **2012**, *51*, 1788–1794. [CrossRef]
45. Tempelhahn, A.; Budzier, H.; Krause, V.; Gerlach, G. Shutter-less calibration of uncooled infrared cameras. *J. Sens. Sens. Syst.* **2016**, *5*, 9–16. [CrossRef]
46. Kusnierek, K.; Korsaeth, A. Challenges in using an analog uncooled microbolometer thermal camera to measure crop temperature. *Int. J. Agric. Biol. Eng.* **2014**, *7*, 60–74. [CrossRef]
47. Lin, D.; Maas, H.-G.; Westfeld, P.; Budzier, H.; Gerlach, G. An advanced radiometric calibration approach for uncooled thermal cameras. *Photogramm. Rec.* **2018**, *33*, 30–48. [CrossRef]
48. Ribeiro-Gomes, K.; Hernández-López, D.; Ortega, J.F.; Ballesteros, R.; Poblete, T.; Moreno, M.A. Uncooled Thermal Camera Calibration and Optimization of the Photogrammetry Process for UAV Applications in Agriculture. *Sensors* **2017**, *17*, 2173. [CrossRef]
49. Gerhards, M.; Schlerf, M.; Mallick, K.; Udelhoven, T. Challenges and Future Perspectives of Multi-/Hyperspectral Thermal Infrared Remote Sensing for Crop Water-Stress Detection: A Review. *Remote Sens.* **2019**, *11*, 1240. [CrossRef]
50. Wan, Q.; Smigaj, M.; Brede, B.; Kooistra, L. Optimizing UAV-based uncooled thermal cameras in field conditions for precision agriculture. *Int. J. Appl. Earth Obs. Geoinf.* **2024**, *134*, 104184. [CrossRef]
51. Chrzanowski, K. Influence of object-system distance on accuracy of remote temperature measurement with IR systems. *Infrared Phys. Technol.* **1995**, *36*, 703–713. [CrossRef]

52. Zhang, Y.-C.; Chen, Y.-M.; Fu, X.-B.; Luo, C. A method for reducing the influence of measuring distance on infrared thermal imager temperature measurement accuracy. *Appl. Therm. Eng.* **2016**, *100*, 1095–1101. [CrossRef]
53. Minkina, W.; Dudzik, S. *Infrared Thermography: Errors and Uncertainties*; John Wiley & Sons: Chichester, UK, 2009. [CrossRef]
54. Westoby, M.J.; Brasington, J.; Glasser, N.F.; Hambrey, M.J.; Reynolds, J.M. 'Structure-from-Motion' photogrammetry: A low-cost, effective tool for geoscience applications. *Geomorphology* **2012**, *179*, 300–314. [CrossRef]
55. Sona, G.; Pinto, L.; Pagliari, D.; Passoni, D.; Gini, R. Experimental analysis of different software packages for orientation and digital surface modelling from UAV images. *Earth Sci. Inform.* **2014**, *7*, 97–107. [CrossRef]
56. Lowe, D.G. Distinctive Image Features from Scale-Invariant Keypoints. *Int. J. Comput. Vis.* **2004**, *60*, 91–110. [CrossRef]
57. Schönberger, J.L.; Frahm, J.-M. Structure-From-Motion Revisited. In Proceedings of the IEEE Conference on Computer Vision and Pattern Recognition (CVPR), Las Vegas, NV, USA, 27–30 June 2016; pp. 4104–4113. [CrossRef]
58. James, M.R.; Robson, S. Straightforward reconstruction of 3D surfaces and topography with a camera: Accuracy and geoscience application. *J. Geophys. Res. Earth Surf.* **2012**, *117*, F03017. [CrossRef]
59. Smith, M.W.; Carrivick, J.L.; Quincey, D.J. Structure from Motion Photogrammetry in Physical Geography. *Prog. Phys. Geogr.* **2016**, *40*, 247–275. [CrossRef]
60. Turner, D.; Lucieer, A.; Malenovský, Z.; King, D.H.; Robinson, S.A. Spatial Co-Registration of Ultra-High Resolution Visible, Multispectral and Thermal Images Acquired with a Micro-UAV over Antarctic Moss Beds. *Remote Sens.* **2014**, *6*, 4003–4024. [CrossRef]
61. Yang, Y.; Lee, X. Four-band Thermal Mosaicking: A New Method to Process Infrared Thermal Imagery of Urban Landscapes from UAV Flights. *Remote Sens.* **2019**, *11*, 1365. [CrossRef]
62. Szeliski, R. Image Alignment and Stitching: A Tutorial. *Found. Trends Comput. Graph. Vis.* **2006**, *2*, 1–104. [CrossRef]
63. Honkavaara, E.; Rosnell, T.; Oliveira, R.; Tommaselli, A. Band registration of tuneable frame format hyperspectral UAV imagers in complex scenes. *ISPRS J. Photogramm. Remote Sens.* **2017**, *134*, 96–109. [CrossRef]
64. Ghassemian, H. A review of remote sensing image fusion methods. *Inf. Fusion* **2016**, *32*, 75–89. [CrossRef]
65. Eisenbeiß, H. UAV Photogrammetry. Ph.D. Thesis, ETH Zurich, Zurich, Switzerland, 2009.
66. Jaud, M.; Passot, S.; Le Bivic, R.; Delacourt, C.; Grandjean, P.; Le Dantec, N. Assessing the Accuracy of High-Resolution Digital Surface Models Computed by PhotoScan and MicMac in Sub-Optimal Survey Conditions. *Remote Sens.* **2016**, *8*, 465. [CrossRef]
67. Štroner, M.; Urban, R.; Línková, L. Photogrammetry Using UAV-Mounted GNSS RTK: Georeferencing Strategies without GCPs. *Remote Sens.* **2021**, *13*, 1336. [CrossRef]
68. Liu, X.; Lian, X.; Yang, W.; Wang, F.; Han, Y.; Zhang, Y. Accuracy Assessment of a UAV Direct Georeferencing Method and Impact of the Configuration of Ground Control Points. *Drones* **2022**, *6*, 30. [CrossRef]
69. Goldman, D.B. Vignette and Exposure Calibration and Compensation. *IEEE Trans. Pattern Anal. Mach. Intell.* **2010**, *32*, 2276–2288. [CrossRef]
70. Wierzbicki, D.; Kedzierski, M.; Fryskowska, A. Assessment of the Influence of UAV Image Quality on the Orthophoto Production. *Int. Arch. Photogramm. Remote Sens. Spat. Inf. Sci.* **2015**, *XL-1/W4*, 1–8. [CrossRef]
71. American Society for Photogrammetry and Remote Sensing (ASPRS). ASPRS Positional Accuracy Standards for Digital Geospatial Data (Edition 1, Version 1.0—November 2014). *Photogramm. Eng. Remote Sens.* **2015**, *81*, A1–A26. [CrossRef]
72. Whitehead, K.; Hugenholtz, C.H. Applying ASPRS Accuracy Standards to Surveys from Small Unmanned Aircraft Systems (UAS). *Photogramm. Eng. Remote Sens.* **2015**, *81*, 787–793. [CrossRef]
73. Huang, Y.; Miyazaki, T.; Liu, X.; Omachi, S. Infrared Image Super-Resolution: Systematic Review, and Future Trends. *arXiv* **2022**, arXiv:2212.12322. [CrossRef]
74. Dash, P.; Göttsche, F.-M.; Olesen, F.-S.; Fischer, H. Land Surface Temperature and Emissivity Estimation from Passive Sensor Data: Theory and Practice-Current Trends. *Int. J. Remote Sens.* **2002**, *23*, 2563–2594. [CrossRef]
75. Tardy, B.; Rivalland, V.; Huc, M.; Hagolle, O.; Marcq, S.; Boulet, G. A Software Tool for Atmospheric Correction and Surface Temperature Estimation of Landsat Infrared Thermal Data. *Remote Sens.* **2016**, *8*, 696. [CrossRef]
76. Van de Griend, A.A.; Owe, M. On the Relationship between Thermal Emissivity and the Normalized Difference Vegetation Index for Natural Surfaces. *Int. J. Remote Sens.* **1993**, *14*, 1119–1131. [CrossRef]
77. Gillespie, A.R.; Rokugawa, S.; Matsunaga, T.; Cothern, J.S.; Hook, S.J.; Kahle, A.B. A Temperature and Emissivity Separation Algorithm for Advanced Spaceborne Thermal Emission and Reflection Radiometer (ASTER) Images. *IEEE Trans. Geosci. Remote Sens.* **1998**, *36*, 1113–1126. [CrossRef]
78. Salisbury, J.W.; D'Aria, D.M. Emissivity of Terrestrial Materials in the 8–14 μm Atmospheric Window. *Remote Sens. Environ.* **1992**, *42*, 83–106. [CrossRef]
79. Kimes, D.S. Azimuthal Radiometric Temperature Measurements of Wheat Canopies. *Appl. Opt.* **1981**, *20*, 1119–1121. [CrossRef]
80. *JCGM 100:2008*; Evaluation of Measurement Data—Guide to the Expression of Uncertainty in Measurement. JCGM: Sèvres, France, 2008. [CrossRef]

81. Willmott, C.J.; Matsuura, K. Advantages of the mean absolute error (MAE) over the root mean square error (RMSE) in assessing average model performance. *Clim. Res.* **2005**, *30*, 79–82. [CrossRef]
82. Possolo, A.; Iyer, H.K. Invited Article: Concepts and tools for the evaluation of measurement uncertainty. *Rev. Sci. Instrum.* **2017**, *88*, 011301. [CrossRef]
83. Gardner, B.R.; Nielsen, D.C.; Shock, C.C. Infrared Thermometry and the Crop Water Stress Index. II. Sampling procedures and interpretation. *J. Prod. Agric.* **1992**, *5*, 466–475. [CrossRef]
84. Farrance, I.; Frenkel, R. Uncertainty of Measurement: A Review of the Rules for Calculating Uncertainty Components through Functional Relationships. *Clin. Biochem. Rev.* **2012**, *33*, 49–75. [PubMed]
85. Fokaides, P.A.; Kalogirou, S.A. Application of infrared thermography for the determination of the overall heat transfer coefficient (U-value) in building envelopes. *Appl. Energy* **2011**, *88*, 4358–4365. [CrossRef]
86. Berni, J.A.J.; Zarco-Tejada, P.J.; Suárez, L.; Fereres, E. Thermal and Narrowband Multispectral Remote Sensing for Vegetation Monitoring from an Unmanned Aerial Vehicle. *IEEE Trans. Geosci. Remote Sens.* **2009**, *47*, 722–738. [CrossRef]
87. Gago, J.; Douthe, C.; Coopman, R.E.; Gallego, P.P.; Ribas-Carbo, M.; Flexas, J.; Escalona, J.; Medrano, H. UAVs challenge to assess water stress for sustainable agriculture. *Agric. Water Manag.* **2015**, *153*, 9–19. [CrossRef]
88. Idso, S.B.; Jackson, R.D.; Pinter, P.J.; Reginato, R.J.; Hatfield, J.L. Normalizing the stress-degree-day parameter for environmental variability. *Agric. Meteorol.* **1981**, *24*, 45–55. [CrossRef]
89. Jackson, R.D.; Idso, S.B.; Reginato, R.J.; Pinter, P.J. Canopy temperature as a crop water stress indicator. *Water Resour. Res.* **1981**, *17*, 1133–1138. [CrossRef]
90. Jones, H.G. Use of infrared thermometry for estimation of stomatal conductance as a possible aid to irrigation scheduling. *Agric. For. Meteorol.* **1999**, *95*, 139–149. [CrossRef]
91. Bellvert, J.; Zarco-Tejada, P.J.; Girona, J.; Fereres, E. Mapping crop water stress index in a 'Pinot-noir' vineyard: Comparing ground measurements with thermal remote sensing imagery from an unmanned aerial vehicle. *Precis. Agric.* **2014**, *15*, 361–376. [CrossRef]
92. Hoffmann, H.; Jensen, R.; Thomsen, A.; Nieto, H.; Rasmussen, J.; Friborg, T. Crop water stress maps for an entire growing season from visible and thermal UAV imagery. *Biogeosciences* **2016**, *13*, 6545–6563. [CrossRef]
93. Romero, M.; Luo, Y.; Su, B.; Fuentes, S. Vineyard water status estimation using multispectral imagery from an UAV platform and machine learning algorithms for irrigation scheduling management. *Comput. Electron. Agric.* **2018**, *147*, 109–117. [CrossRef]
94. Sishodia, R.P.; Ray, R.L.; Singh, S.K. Applications of Remote Sensing in Precision Agriculture: A Review. *Remote Sens.* **2020**, *12*, 3136. [CrossRef]
95. Adão, T.; Hruška, J.; Pádua, L.; Bessa, J.; Peres, E.; Morais, R.; Sousa, J.J. Hyperspectral Imaging: A Review on UAV-Based Sensors, Data Processing and Applications for Agriculture and Forestry. *Remote Sens.* **2017**, *9*, 1110. [CrossRef]
96. Aasen, H.; Honkavaara, E.; Lucieer, A.; Zarco-Tejada, P.J. Quantitative Remote Sensing at Ultra-High Resolution with UAV Spectroscopy: A Review of Sensor Technology, Measurement Procedures, and Data Correction Workflows. *Remote Sens.* **2018**, *10*, 1091. [CrossRef]
97. Mesas-Carrascosa, F.J.; Verdú Santano, D.; Meroño, J.E.; Sánchez de la Orden, M.; García-Ferrer, A. Open source hardware to monitor environmental parameters in precision agriculture. *Biosyst. Eng.* **2015**, *137*, 73–83. [CrossRef]
98. Dugdale, S.J.; Kelleher, C.A.; Malcolm, I.A.; Caldwell, S.; Hannah, D.M. Assessing the potential of drone-based thermal infrared imagery for quantifying river temperature heterogeneity. *Hydrol. Process.* **2019**, *33*, 1152–1163. [CrossRef]
99. Torgersen, C.E.; Faux, R.N.; McIntosh, B.A.; Poage, N.J.; Norton, D.J. Airborne thermal remote sensing for water temperature assessment in rivers and streams. *Remote Sens. Environ.* **2001**, *76*, 386–398. [CrossRef]
100. Handcock, R.N.; Gillespie, A.R.; Cherkauer, K.A.; Kay, J.E.; Burges, S.J.; Kampf, S.K. Accuracy and uncertainty of thermal-infrared remote sensing of stream temperatures at multiple spatial scales. *Remote Sens. Environ.* **2006**, *100*, 427–440. [CrossRef]
101. Lewandowski, J.; Meinikmann, K.; Ruhtz, T.; Pöschke, F.; Kirillin, G. Localization of lacustrine groundwater discharge (LGD) by airborne measurement of thermal infrared radiation. *Remote Sens. Environ.* **2013**, *138*, 119–125. [CrossRef]
102. Lee, E.; Yoon, H.; Hyun, S.P.; Burnett, W.C.; Koh, D.; Ha, K.; Kim, D.; Kim, Y.; Kang, K. Unmanned aerial vehicles (UAVs)-based thermal infrared (TIR) mapping, a novel approach to assess groundwater discharge into the coastal zone. *Limnol. Oceanogr. Methods* **2016**, *14*, 725–735. [CrossRef]
103. Dugdale, S.J.; Hannah, D.M.; Malcolm, I.A. River temperature modelling: A review of process-based approaches and future directions. *Earth-Sci. Rev.* **2017**, *175*, 97–113. [CrossRef]
104. Biggart, M.; Stocker, J.; Doherty, R.M.; Wild, O.; Carruthers, D.; Grimmond, S.; Han, Y.; Fu, P.; Kotthaus, S. Modelling spatiotemporal variations of the canopy layer urban heat island in Beijing at the neighbourhood scale. *Atmos. Chem. Phys.* **2021**, *21*, 13687–13711. [CrossRef]
105. Crawford, B.; Grimmond, C.S.B.; Gabey, A.; Marconcini, M.; Ward, H.C.; Kent, C.W. Variability of urban surface temperatures and implications for aerodynamic energy exchange in unstable conditions. *Q. J. R. Meteorol. Soc.* **2018**, *144*, 1719–1741. [CrossRef]
106. Oke, T.R. The energetic basis of the urban heat island. *Q. J. R. Meteorol. Soc.* **1982**, *108*, 1–24. [CrossRef]

107. Weng, Q.; Lu, D.; Schubring, J. Estimation of land surface temperature–vegetation abundance relationship for urban heat island studies. *Remote Sens. Environ.* **2004**, *89*, 467–483. [CrossRef]
108. Stewart, I.D.; Oke, T.R. Local Climate Zones for Urban Temperature Studies. *Bull. Am. Meteorol. Soc.* **2012**, *93*, 1879–1900. [CrossRef]
109. Henn, K.A.; Peduzzi, A. Surface Heat Monitoring with High-Resolution UAV Thermal Imaging: Assessing Accuracy and Applications in Urban Environments. *Remote Sens.* **2024**, *16*, 930. [CrossRef]
110. Zhang, D.; Zhan, C.; Chen, L.; Wang, Y.; Li, G. Review of unmanned aerial vehicle infrared thermography (UAV-IRT) applications in building thermal performance: Towards the thermal performance evaluation of building envelope. *Quant. InfraRed Thermogr. J.* **2025**, *22*, 266–296. [CrossRef]
111. Balaras, C.A.; Argiriou, A.A. Infrared thermography for building diagnostics. *Energy Build.* **2002**, *34*, 171–183. [CrossRef]
112. Tomita, K.; Chew, M.Y.L. A Review of Infrared Thermography for Delamination Detection on Infrastructures and Buildings. *Sensors* **2022**, *22*, 423. [CrossRef]
113. Quater, P.B.; Grimaccia, F.; Leva, S.; Mussetta, M.; Aghaei, M. Light Unmanned Aerial Vehicles (UAVs) for Cooperative Inspection of PV Plants. *IEEE J. Photovolt.* **2014**, *4*, 1107–1113. [CrossRef]
114. Omar, T.; Nehdi, M.L. Remote sensing of concrete bridge decks using unmanned aerial vehicle infrared thermography. *Autom. Constr.* **2017**, *83*, 360–371. [CrossRef]
115. Sabry, A.H.; Bıyıkoğlu, A.; Camdali, U. A comprehensive review of unmanned aerial vehicle-based thermal imaging and deep learning for PV power plant anomaly detection and performance assessment. *Eng. Appl. Artif. Intell.* **2026**, *163*, 113070. [CrossRef]
116. Thompson, J.; Giovanini, E.; Befus, K.; Marshall, E.; Allison, C. The use of UAV-based visible and multispectral thermal infrared data for active volcano monitoring and analysis: Test of a low-cost solution applied to the 2022 Meradalir eruption. *Volcanica* **2025**, *8*, 325–339. [CrossRef]
117. Watts, A.C.; Ambrosia, V.G.; Hinkley, E.A. Unmanned Aircraft Systems in Remote Sensing and Scientific Research: Classification and Considerations of Use. *Remote Sens.* **2012**, *4*, 1671–1692. [CrossRef]
118. Merino, L.; Caballero, F.; Martínez-de-Dios, J.R.; Maza, I.; Ollero, A. An Unmanned Aircraft System for Automatic Forest Fire Monitoring and Measurement. *J. Intell. Robot. Syst.* **2012**, *65*, 533–548. [CrossRef]
119. Dugdale, S.J. A practitioner's guide to thermal infrared remote sensing of rivers and streams: Recent advances, precautions and considerations. *WIREs Water* **2016**, *3*, 251–268. [CrossRef]
120. Bagavathiappan, S.; Lahiri, B.B.; Saravanan, T.; Philip, J.; Jayakumar, T. Infrared thermography for condition monitoring—A review. *Infrared Phys. Technol.* **2013**, *60*, 35–55. [CrossRef]
121. *ISO 6781-3:2015*; Performance of Buildings—Detection of Heat, Air and Moisture Irregularities in Buildings by Infrared Methods—Part 3: Qualifications of Equipment Operators, Data Analysts and Report Writers. International Organization for Standardization: Geneva, Switzerland, 2015.
122. *ASTM E1933-14*; Standard Practice for Measuring and Compensating for Emissivity Using Infrared Imaging Radiometers. ASTM International: West Conshohocken, PA, USA, 2014. [CrossRef]
123. Zhang, L.; Zhang, L.; Du, B. Deep Learning for Remote Sensing Data: A Technical Tutorial on the State of the Art. *IEEE Geosci. Remote Sens. Mag.* **2016**, *4*, 22–40. [CrossRef]
124. Zhu, X.X.; Tuia, D.; Mou, L.; Xia, G.-S.; Zhang, L.; Xu, F.; Fraundorfer, F. Deep Learning in Remote Sensing: A Comprehensive Review and List of Resources. *IEEE Geosci. Remote Sens. Mag.* **2017**, *5*, 8–36. [CrossRef]
125. Goodfellow, I.J.; Pouget-Abadie, J.; Mirza, M.; Xu, B.; Warde-Farley, D.; Ozair, S.; Courville, A.; Bengio, Y. Generative Adversarial Nets. In *Advances in Neural Information Processing Systems 27 (NeurIPS 2014)*; Neural Information Processing Systems Foundation, Inc.: San Diego, CA, USA, 2014; pp. 2672–2680.
126. Ledig, C.; Theis, L.; Huszár, F.; Caballero, J.; Cunningham, A.; Acosta, A.; Aitken, A.P.; Tejani, A.; Totz, J.; Wang, Z.; et al. Photo-Realistic Single Image Super-Resolution Using a Generative Adversarial Network. In *Proceedings of the IEEE Conference on Computer Vision and Pattern Recognition (CVPR)*; IEEE: New York, NY, USA, 2017; pp. 4681–4690. [CrossRef]
127. Dong, C.; Loy, C.C.; He, K.; Tang, X. Image Super-Resolution Using Deep Convolutional Networks. *IEEE Trans. Pattern Anal. Mach. Intell.* **2016**, *38*, 295–307. [CrossRef]
128. Shi, W.; Caballero, J.; Huszár, F.; Totz, J.; Aitken, A.P.; Bishop, R.; Rueckert, D.; Wang, Z. Real-Time Single Image and Video Super-Resolution Using an Efficient Sub-Pixel Convolutional Neural Network. In *Proceedings of the IEEE Conference on Computer Vision and Pattern Recognition (CVPR)*; IEEE: New York, NY, USA, 2016; pp. 1874–1883. [CrossRef]
129. Mittal, S. A Survey on Optimized Implementation of Deep Learning Models on the NVIDIA Jetson Platform. *J. Syst. Archit.* **2019**, *97*, 428–442. [CrossRef]
130. Redmon, J.; Farhadi, A. YOLOv3: An Incremental Improvement. *arXiv* **2018**, arXiv:1804.02767. [CrossRef]
131. Maes, W.H. Practical Guidelines for Performing UAV Mapping Flights with Snapshot Sensors. *Remote Sens.* **2025**, *17*, 606. [CrossRef]

132. Wang, Z.; Zhou, J.; Ma, J.; Wang, Y.; Liu, S.; Ding, L.; Tang, W.; Pakezhamu, N.; Meng, L. Removing Temperature Drift and Temporal Variation in Thermal Infrared Images of a UAV Uncooled Thermal Infrared Imager. *ISPRS J. Photogramm. Remote Sens.* **2023**, *203*, 392–411. [CrossRef]
133. Burke, C.; Rashman, M.F.; Wich, S.; Symons, A.; Theron, C.; Longmore, S. Optimizing Observing Strategies for Monitoring Animals Using Drone-Mounted Thermal Infrared Cameras. *Int. J. Remote Sens.* **2019**, *40*, 439–467. [CrossRef]

Disclaimer/Publisher's Note: The statements, opinions and data contained in all publications are solely those of the individual author(s) and contributor(s) and not of MDPI and/or the editor(s). MDPI and/or the editor(s) disclaim responsibility for any injury to people or property resulting from any ideas, methods, instructions or products referred to in the content.